



HAL
open science

Influence of point defects and grain boundaries on plasticity and phase transition in uniaxially-compressed iron

N. Amadou, T. de Resseguier, A. Dragon

► **To cite this version:**

N. Amadou, T. de Resseguier, A. Dragon. Influence of point defects and grain boundaries on plasticity and phase transition in uniaxially-compressed iron. *Computational Condensed Matter*, 2021, 27, pp.e00560. 10.1016/j.cocom.2021.e00560 . hal-03430918

HAL Id: hal-03430918

<https://hal.science/hal-03430918>

Submitted on 16 Nov 2021

HAL is a multi-disciplinary open access archive for the deposit and dissemination of scientific research documents, whether they are published or not. The documents may come from teaching and research institutions in France or abroad, or from public or private research centers.

L'archive ouverte pluridisciplinaire **HAL**, est destinée au dépôt et à la diffusion de documents scientifiques de niveau recherche, publiés ou non, émanant des établissements d'enseignement et de recherche français ou étrangers, des laboratoires publics ou privés.

Influence of point defects and grain boundaries on plasticity and phase transition in uniaxially-compressed iron

N. Amadou^{1,2}, T. de Resseguier¹ and A. Dragon¹

¹ Institut Pprime, CNRS, ENSMA, Université de Poitiers, Poitiers, France

² Département de Physique, Université Abdou Moumouni de Niamey, BP. 10662 Niamey, Niger

Abstract

Using MD computations we have reported recently a shear stiffening (hardening-like) effect in [001]-oriented defect-free iron single crystal. This effect makes shift the structural phase transition to a particularly high pressure level under ramp compression, but not under shock compression, so that the question arises about the essential role of the compression path and wave evolution in the solid state response including phase transition. Here, plasticity and phase transition are studied for iron samples under non-equilibrium uniaxial compression. Our focus is put on the effects of grain size and point defects such as atoms vacancy. Consistently with our previous results, it is found that, after yielding via twinning, both defect-free and defective iron single crystals exhibit a hardening-like effect while the twins progressively recede upon further compression and no dislocations activity is detected. This leads to mounting of the deviatoric stress. Yet, the transition onset pressure shift and temperature behavior are found to be defect-density dependent. Considering polycrystalline lattice, plasticity consists in complex interplay of intra-grain twinning and dislocation activities from grain boundaries. The elastic stiffening is attenuated now as compared to single crystal so that the phase transition is found to occur at much lower pressure in polycrystalline iron.

keywords: uniaxial compression, Molecular Dynamics, phase transition, plasticity, iron, lattice defects, twinning, mono-and poly-crystal.

1 Introduction

Since it was first reported more than six decades ago [1], the polymorphic transformation of iron from its bcc structure (α) at ambient conditions to the more compact hcp structure (ε) when compressed above about 13 GPa has been the subject of considerable research work, with various motivations, from geophysics to planetary physics, materials science or engineering applications. A variety of complementary approaches, both experimental and theoretical have been employed, including the detection and analysis of multiple wave structures [2, 3, 4, 5], post-recovery evidence of the $\alpha - \varepsilon - \alpha$ cycle [6, 7], in-situ X-ray diffraction (XRD) [8, 9], extended X-ray absorption fine structure (EXAFS) [10, 11], non-equilibrium molecular dynamics (NEMD) [12, 13, 14, 15], and first principle calculations [16]. Key issues have been investigated, such as the mechanisms governing this transformation, but some essential questions remain open, and somewhat controversial. Thus, the transition to an intermediate, metastable, possibly short-lived fcc-structure before the final hcp phase has been suggested [12, 13] or excluded [17, 16]. The role of strain rate effects in dynamic compression experiments, under both shock and ramp-loading, and their influence on the transition onset pressure are still unclear [3, 4, 5]. The absence [18] or occurrence of shock-induced plasticity [19, 20, 21], either twin-induced [22, 23] or dislocation-dominated [15], depending on orientation [24] and pre-existing 'defects' [25, 26], grain boundaries [27, 28] or initial dislocations [29], have also been widely debated, as well as possible coupling of such plasticity with phase transition [30, 27, 31, 32, 23, 29].

Over the past few years, we have used molecular dynamics to investigate the response of single crystal iron to fast, piston-driven, both shock and ramp compression, with a special attention to the

coupling between the bcc-hcp transformation and plastic processes, either twinning [23] or orientation-dependent dislocation slip at higher initial temperatures [33]. A striking form of such coupling was evidenced as an 'elastic stiffening' of the bcc matrix upon ramp compression above the twinning pressure, leading to a confining effect which was shown to inhibit the nucleation and growth of hcp embryos, thus shifting the transition onset pressure to very high values. In this paper, we simulate high rate homogeneous uniaxial compression [30, 34] of both single-crystal with or without atoms vacancies and polycrystalline iron with various grain size. Unlike in piston-driven loading, wave propagation is disregarded since the whole sample is deformed at each time step. This allows exploring at the atomic scale the overall response to non-equilibrium uniaxial compression, with focus on the specific role of grain boundaries and material defects on plasticity and phase transformation, to provide further insight into some aforementioned questions. In particular, depending on the grain number, polycrystalline samples are shown to exhibit complex interplay of intra-grain twinning and dislocation activities from grain boundaries, which strongly affects thermo-mechanical behavior and subsequent phase transition.

2 Methods

Non-equilibrium MD simulations were realized using the Large-scale Atomic/Molecular Massively Parallel Simulator (LAMMPS) code [35]. The simulations were realized in the NVE ensemble while the interactions between atoms were modeled through the embedded atom model formalism [36, 37]. The iron model was the modified version of the Ackland potential [30] to account for both plasticity and phase transformation [27, 38, 23, 33].

Samples with 8 millions atoms, representing six different initial microstructures, were simulated at 50 K initial temperature. These samples could be classified into two categories. The first consists of [001]-oriented single crystals with or without defects ($\approx 29 \times 29 \times 115 \text{ nm}^3$ size). Defects were introduced by randomly removing $p\%$ atoms from the perfect lattice, with p ranging from 0.12 to 0.57. The second category was polycrystalline samples ($\approx 46 \times 46 \times 46 \text{ nm}^3$ size) with grain number of 4 (size range $\approx 24\text{-}32 \text{ nm}$), 24 (size range $\approx 13\text{-}20 \text{ nm}$) and 124 (size range $\approx 6\text{-}13 \text{ nm}$). They were obtained by Voronoi tessellation method using the AtomsK package [39]. Then, the grain boundaries potential energy was minimized following a thermal annealing procedure simulation similar to [13] where the samples were equilibrated at 600 K during 15 ps then cooled during 15 ps.

Both categories of samples were uniaxially deformed along the z-direction with periodic boundary conditions in the three directions. Deformation was incremented at each time step, leading to a strain rate of about $5 \times 10^{12} \text{ s}^{-1}$. This is about three to four orders of magnitude beyond the range that can be reached experimentally under laser-ramp compression, typically 10^8 s^{-1} [21] or under picosecond-laser driven compression, above 10^9 s^{-1} [40]. It is also above the range which we explored previously under piston-driven compression, about $10^8\text{-}10^9 \text{ s}^{-1}$ [23, 33]. Still, the results reported in the present paper show numerous correlations with both experimental observations and MD simulations by various authors, as will be detailed further. Nevertheless, expanding our investigation over a range of lower strain rates (implying higher computational cost) will be the next stage of our ongoing work.

The cubic dimensions of the polycrystalline samples were chosen to capture global effects of grain boundaries distributed in both transverse and longitudinal directions, while an elongated domain was chosen to study the more homogeneous single crystals.

The pressure (i.e. compressive stress) tensor was computed following

$$P_{\alpha\beta} = \frac{\sum_i m_i v_{i\alpha} v_{i\beta}}{V} + \frac{\sum_i r_{i\alpha} F_{i\beta}}{V} \quad (1)$$

where α and β take on values x , y and z , m_i , r_i and v_i are the atomic mass, position and velocity, respectively, F_i is the force on atom i , and V is the system volume. The first term of Eq. 1 represents the momentum flow of an atom i while the second term corresponds to the virial term. Under uniaxial deformation, the compressive stress in the compression direction can be written

$$P_{zz} = (P_{zz} + P_{xx} + P_{yy})/3 + (2P_{zz} - (P_{xx} + P_{yy}))/3 = \bar{P} + 4/3\tau \quad (2)$$

where \bar{P} is the hydrostatic pressure and τ , a shearing stress defined by

$$\tau = \frac{1}{2} \left(P_{zz} - \frac{1}{2}(P_{xx} + P_{yy}) \right) \quad (3)$$

and classically referred to as the shear stress [41, 42, 43]. Next, P_{zz} is noted P_z for brevity. The temperature was computed from the kinetic energy by $\frac{3}{2}nk_B T = \frac{1}{2}m \sum_i \vec{v}_i^2$, where k_B and n are the Boltzmann constant and total number of atoms respectively.

The atomic spatial configurations were analysed using the OVITO software [44], where twins were identified using the centrosymmetry parameter, dislocations were detected with the Dislocation Extraction Algorithm (DXA) tool [45], and the local structural phase analysis was performed by adaptative Common Neighbor Analysis (CNA) [46].

3 Results and Discussion

3.1 Plasticity

Lattice level investigations are fundamental for understanding the mechanisms governing plastic flow in solids. Under high deformation rate, two microprocesses were found to occur in competitive manner: slip of dislocations and twinning deformation [47]. Which one operates in a given deformation state

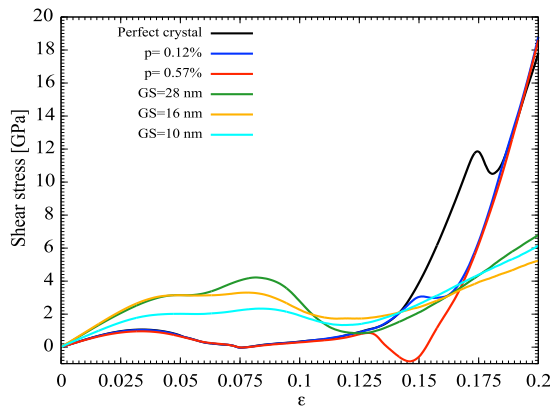


Figure 1: Shear stress versus strain for perfect single crystal (black curve); single crystal with 0.12% (blue curve) and 0.57% (red curve) of vacancy defects and polycrystalline iron with grain size (GS) of about 28 nm (forest-green curve), about 16 nm (orange curve) and about 10 nm (cyan curve).

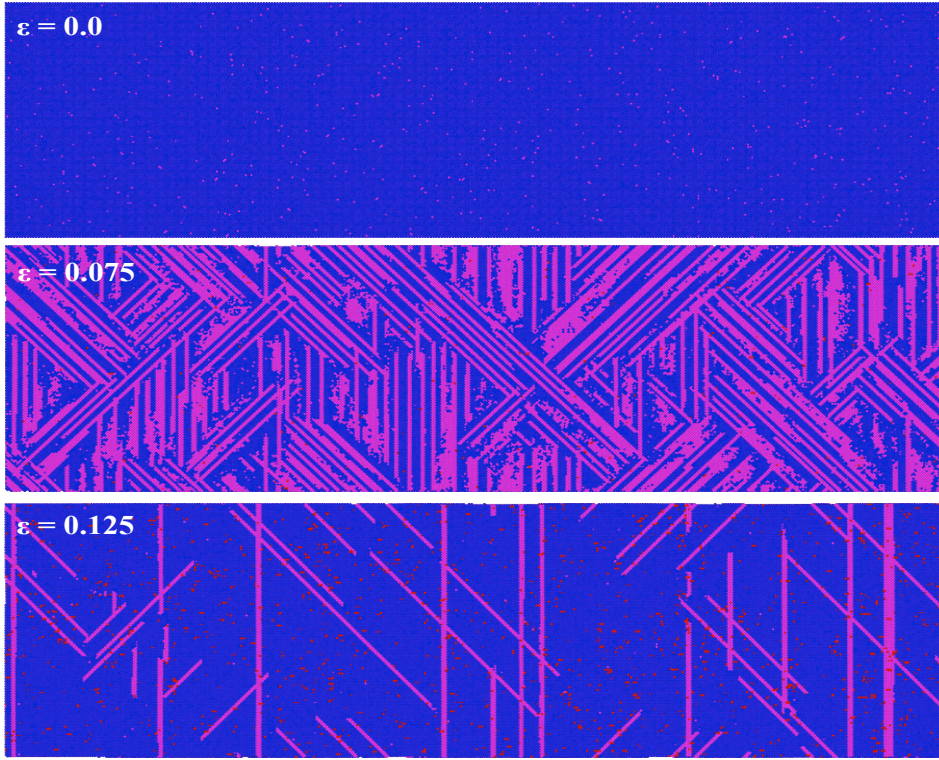


Figure 2: Atomic rearrangements associated with plastic deformation at different strain in initially defect-free iron single crystal, detected by centrosymmetry analysis. For strains up to 0.075, atoms form structures that correspond to twins (magenta). Above 0.075 strain, the twins recede upon further compression, with a new increase of the shear stress. A similar behavior was observed for the defective initial conditions. See text for details.

depends on strain rate, temperature and crystal initial conditions (crystal purity, microstructure etc.). Thus, it was suggested from experimental results that understanding the iron elastic to plastic response requires an exhaustive investigation of how the initial crystal state affects the response and final state [14].

Atomistic simulations are particularly suited to investigate these questions as they are expected to accurately capture every possible mechanism of material response [48, 49]. Here we are specifically interested in the effects of the initial microstructure: how vacancy defects and grain size determine the path and the underlying microprocess of plastic deformation. Fig. 1 shows the shear stress versus strain during the uniaxial compression for various samples (throughout this paper, ε stands for ε_{zz} , all other components of the strain tensor being zero). For perfect and defective single crystalline iron, the shear stress increases linearly to a value of 1 GPa at strain of about 0.03 where plastic flow activities start. The defects associated with the plastic deformation are analysed using both DXA tool and centrosymmetry parameter. While no dislocations are found by the DXA analysis, two-dimensional planar defects are detected by the centrosymmetry analysis (Fig. 2 and Fig. 3), which are identified to be twins (Fig. 4). The twins nucleation leads to a saturation in the shear stress, until the strain reaches about 0.04. Then, the twins start to grow rapidly inducing a fast relaxation of the shear stress. At strain of about 0.064, the shear stress is almost fully relaxed and twins growth slows down. When the strain reaches a value around 0.08, a decrease in the twins density is observed. Due to the subsequent hardening-like effect, also observed under ramp compression [23], the shear stress starts to increase

again with growing strain, until the onset of the structural phase transition at strain values of 0.168, 0.152 and 0.122 for the defect-free, $p = 0.12\%$ and $p = 0.57\%$ defective crystal respectively. The plastic deformation was observed here to be specifically mediated by twinning and no dislocations activities were detected. Also, no effect of the vacancy defect was observed on the elastic-plastic response until the structural phase transition occurs (see sec. 3.2). One may argue that the lack of dislocations is probably associated with the extremely high strain rate used in our simulations. However, even at much lower strain rate on the order of 10^8 s^{-1} , the kinetics of dislocations for this direction has been found to be extremely slow; hence the plastic deformation remains dominated by twinning deformation [33]. This contrasts with recent MD results obtained with the same potential for iron where the inclusion of carbon impurities was found to lower the Hugoniot elastic limit of Fe-C [50].

In the case of polycrystalline iron samples, intra-grain twinning similar to that occurring in the single crystal case is observed (Fig. 5 and Fig. 6). In addition, an important plastic work comes from the generation, multiplication and propagation of dislocations from grain boundaries, in consistence with previous work [30]. Thus, the combination of these plasticity modes bounds the shear stress at 3.5 and 2 GPa for larger grain sizes (about 13-30 nm) and smaller ones (about 6-13 nm), respectively. Then, at strain around 0.06 the intra-grain elastic stiffness leads to an increase in the shear stress. The larger the grain size, the more dominant the grain elastic stiffness contribution.

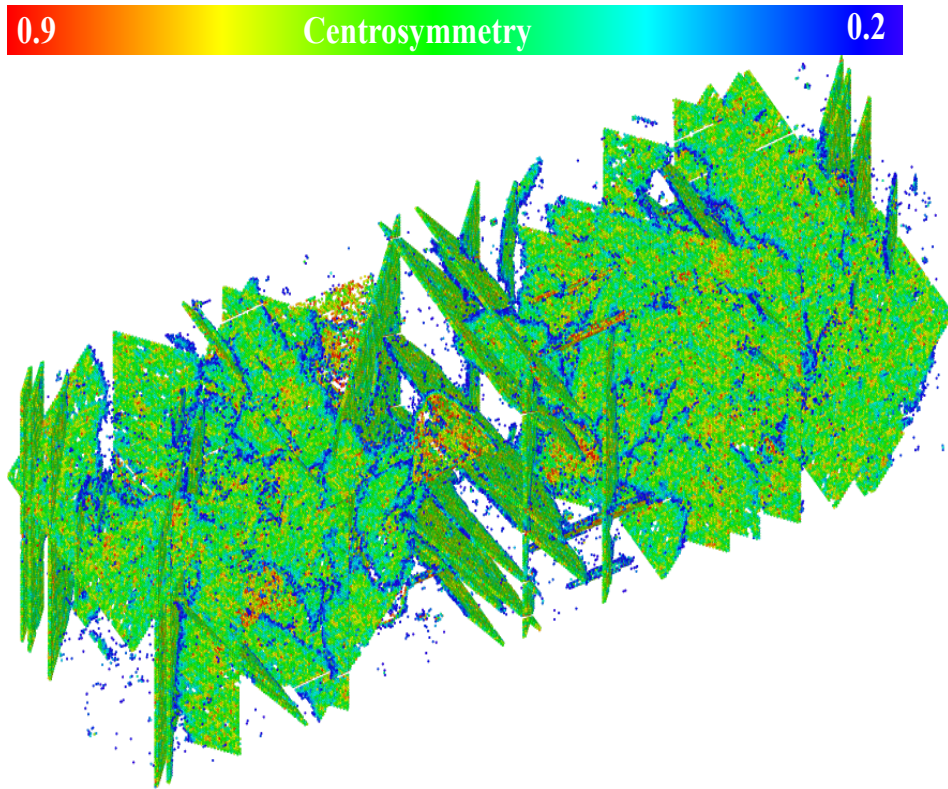


Figure 3: Perspective view of the defects associated with plastic deformation, detected by centrosymmetry analysis, in a single crystal of initial proportion $p = 0.12\%$ of atom vacancies subjected to uniaxial compression to a 0.125 strain. Only defective atoms are shown, colored according to their centrosymmetric parameter.

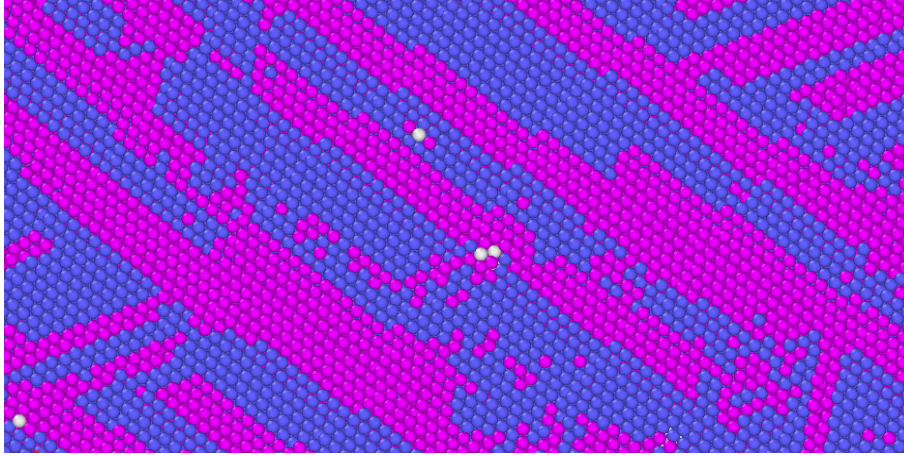


Figure 4: Example of atoms configuration in the (112) plane in the $p = 0.12\%$ defective crystal at strain of 0.075. Violet colored atoms (nocentrosymmetrics) correspond to planar defects of finite width and a mirror symmetry with respect to the surrounding blue structure (centrosymmetric atoms). These defects are associated with twins.

3.2 Structural phase transition

Solid-solid phase transformation in a crystal involves a reorganization of atomic configuration in space. In iron such transformations are of martensitic-type, i.e. temperature driven and are well represented by classical theory of nucleation and growth. Here, suitable thermal fluctuations provide a small number of atoms with sufficient activation energy to transform in the vicinity of some favorable sites (in real material these sites called 'germ nuclei' are supposed to pre-exist in the parent phase) to form a small nucleus of the new phase. Then these nuclei grow at the expense of the parent matrix until almost the whole structure is transformed. The thermodynamic driving force for this process results from the negative bulk (chemical) free energy difference between the initial and final configurations. However, the formation of nucleus induces positive interface energy, which opposes the transformation. Besides, as the product and parent phases have different crystalline structures and specific volumes,

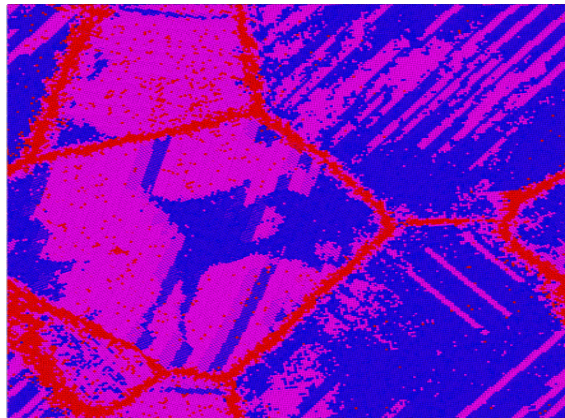


Figure 5: Atomic configurations associated with plastic deformation detected by centrosymmetry analysis in polycrystalline iron with grains of about 28 nm at a strain of 0.055 corresponding to P_z of 13 GPa. Twinned atoms are colored in magenta, red atoms belong to grain boundaries.

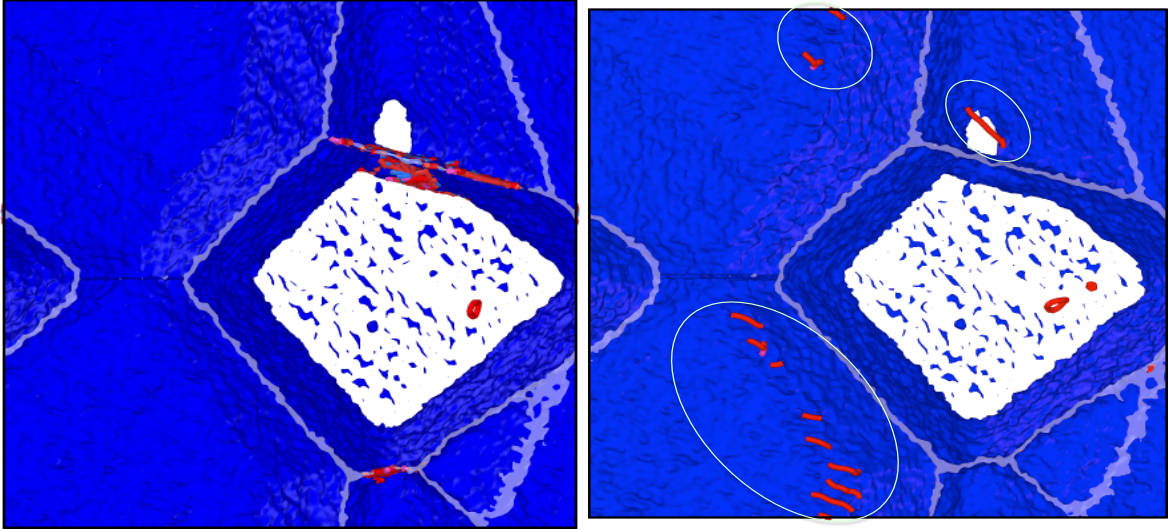


Figure 6: DXA analysis showing grain boundaries (blue walls) and dislocations (red lines) at $\varepsilon = 0.0$ (left) and $\varepsilon = 0.05$ corresponding to $P_z \approx 13$ GPa (right). The elliptic contours point to new, intra-grain dislocations emitted from grain boundaries, i.e plastic strain in the bcc phase.

the transformation is accompanied by dimensional changes. Changes in volume and shape cannot occur freely because of the rigidity of the surrounding matrix, and strain energy is being induced [51]. Like the interface energy, this strain energy works against the transformation and constitutes an important factor in the balance [52]. For nucleus to grow, it must thus reach a critical size where the net free energy balance is still negative. In such model of nucleation and growth, the pre-existing germ

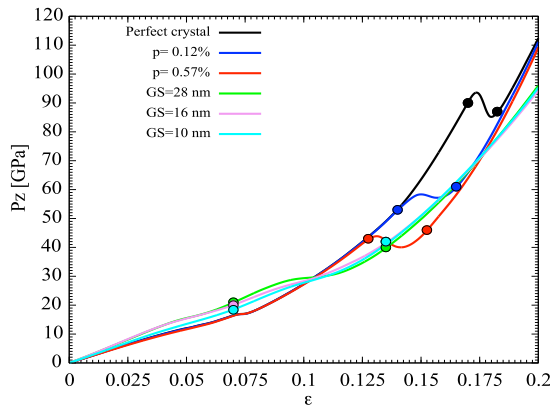


Figure 7: P_z versus strain for perfect single crystal (black curve); defective single crystal with $p = 0.12\%$ (blue curve) and $p = 0.57\%$ (red curve) of vacancy defects and polycrystalline iron with grain size (GS) of about 28 nm (green curve), about 16 nm (violet curve) and about 10 nm (cyan curve). The mixed-phase regimes are delimited by two dots on each curve.

nuclei may consist of grain boundaries, impurities, defects such as vacancies, dislocations or twins, etc. [53, 54]. Thus, varying sample initial microstructure provides valuable information on structural phase transformation. Here, depending on the initial state of the sample, the iron bcc-hcp transition characteristics were found to be very different. Fig. 7, 8 and 9 show P_z , fraction of hcp and temperature versus strain respectively.

Like under ramp compression and in contrast to shock compression [23, 27], the onset pressure for the structural phase transition in single crystal iron (defect-free and defective) was found to be very high due to the elastic stiffening of the bcc matrix leading to a confinement effect on the hcp embryos, requiring strong compression for the structural transformation to take place [23]. Indeed, in the case of defect-free single crystal the transition begins around 90 GPa at strain about 0.17 and the shear stress around 10 GPa. Then follows a stage of rapid growth where the hcp fraction evolves from 10 % to about 80% over strain variation of only $\Delta\varepsilon \approx 0.006$ leading to a mixed regime with strong relaxation (of about 10 GPa) of Pz (see Fig. 7). Due to the high rigidity of the bcc matrix, an important plastic work is necessary to accommodate the product phase. Thus this dissipative process leads to an increase of temperature, which evolves from 100 K at the beginning of the structural phase transformation to about 500 K at its completion ($\Delta T \approx 400K$).

A similar temperature growth was also observed during the structural phase transformation in previous MD simulations of iron single crystal under uniaxial compression using the Voter-Chen potential [34]. It should be pointed out that such significant heating, closely related to plasticity as stated above, is a highly transient, non-equilibrium process [55]. Therefore, it is not incompatible with the negative slope of the P-T phase boundary and corresponding compression path in the iron equilibrium phase diagram (e.g. [56, 57]). In particular, according to this negative slope, the higher the initial sample temperature, the lower the transition onset pressure, which agrees with both ramp compression experiments [57] and MD simulations [33].

Defects act locally to lower free energy which favors the nucleation on these sites, thus occasioning heterogeneous nucleation. Though the elastic stiffening was observed in both defect-free and defective single crystal, accounting for defects leads to a significant effect on the structural phase transition (see Fig. 10). Thus, for the moderate defect proportion (0.12% vacancy defect), the transition was observed at around 50 GPa for strain of about 0.15. This important reduction in transition onset pressure (divided almost by a factor 2 with respect to defect-free crystal) is due to the combined effect

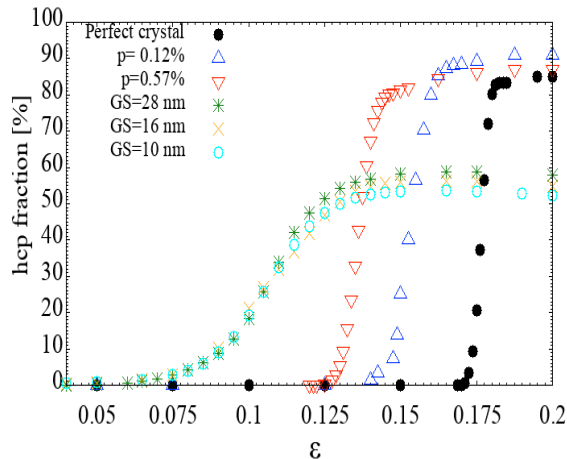


Figure 8: Evolution of the hcp atoms fraction during the compression of perfect single crystal (filled black circle); single crystal with $p = 0.12\%$ (up blue triangle) and 0.57% (down red triangle) of vacancy defects and polycrystalline iron with grain size (GS) about 28 nm (green stars), about 16 nm (orange cross) and about 10 nm (cyan circle)

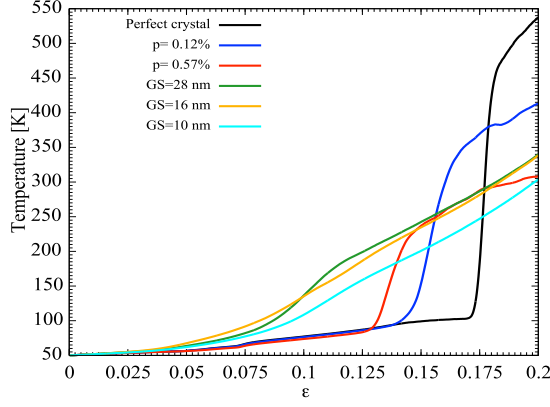


Figure 9: Temperature evolution for perfect single crystal (black curve); single crystal with $p = 0.12\%$ (blue curve) and $p = 0.57\%$ (red curve) of vacancy defects and polycrystalline iron with grain size (GS) about 28 nm (forest-green curve), about 16 nm (orange curve) and about 10 nm (cyan curve).

of heterogeneous nucleation and plasticity. In fact, defects reduce the interface energy contribution to the free energy, thus the nucleation could start at much lower pressure while the bcc matrix is not as rigid as in the case of defect-free sample. The confinement of the product phase embryos was less important and the growth could occur more easily. Here, the shear at the beginning of the transition is 4 GPa. Consequently, the plastic work required to accommodate the product phase is much lower than for the defect-free case and the temperature increase is smaller too, $\Delta T \approx 250K$. Besides, the hcp fraction growth was found to be less rapid than for the single crystal case, probably due to lower temperature and larger mixed regime.

On further increasing the defect density, the nucleation site density increases too and, during the

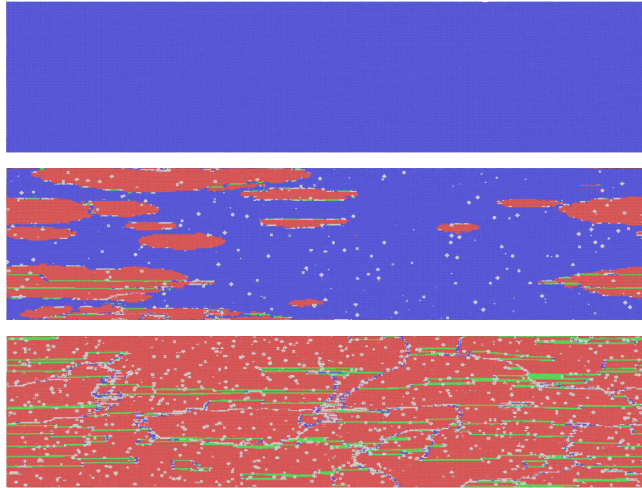


Figure 10: CNA analysis showing the atomic crystallographic structure type at strain $\varepsilon = 0.15$ for iron single crystal. The images from top to bottom are the defect-free (top), defective with $p = 0.12\%$ (middle) and 0.57% (bottom) respectively. The corresponding P_z are 44, 58 and 64 GPa respectively. Bcc atoms are colored blue, fcc green, hcp red and atoms in disordered regions developing around vacancies are colored white. The fraction of these unstructured (white colored) atoms are 1.4 and 6.8 % of the total atoms number for $p = 0.12\%$ and 0.57% respectively

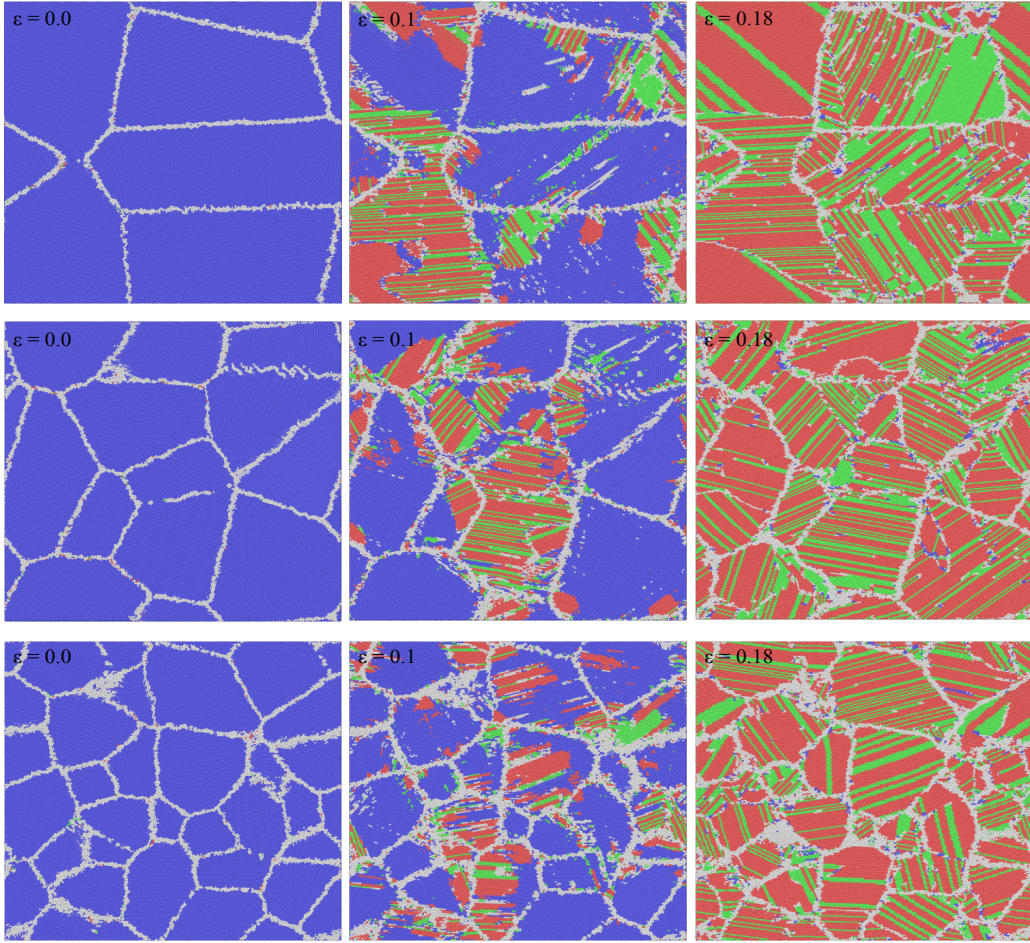


Figure 11: CNA analysis showing the atomic crystallographic structure at different strain, $\varepsilon = 0.0$ (left column, $P_z = 0$ GPa), $\varepsilon = 0.1$ (middle column, $P_z = 28$ GPa) and $\varepsilon = 0.18$ (right column, $P_z = 75$ GPa), for polycrystalline iron with grain size about 28 nm (top row), about 16 nm (center row) and about 10 nm (bottom row), respectively. Bcc atoms are colored blue, fcc green, hcp red and other structure white.

compression, closer nuclei aggregate to form a cluster that becomes thermodynamically stable at much lower pressure. Thus, the higher the defect density, the lower the transition onset pressure. For example, for 0.57% of defects, the onset pressure is around 40 GPa for a strain of about 0.128. For this case, as the onset pressure was moderate, the corresponding shear stress was low, about 1 GPa. The structural phase transition was then able to relax completely the shear stress through the sample during the transformation. Even more interestingly, an over-relaxation was observed, which intensity was more important than previously reported [13, 41, 43, 58, 59]. The temperature increase was also small, $\Delta T \approx 150K$, again due to lower plastic work required to accommodate the product phase. The nucleation was homogeneous in the perfect single crystal while it was heterogeneous for defective single crystal. However, the morphology of nucleon was observed to be same. Fcc phase nuclei were observed to form first, followed by hcp nuclei [34]. Nevertheless, upon compression only hcp nuclei become stable then grow. Their growth was more rapid in (110) and (1 $\bar{1}$ 0) planes than along the perpendicular direction conducting to nuclei of flat shape [12]. This behavior was due to the prominence of the elastic contribution and was also observed for other potential such as the ME potential [12]. For defective sample a small increase of the fcc fraction was observed on increasing the defect density during the

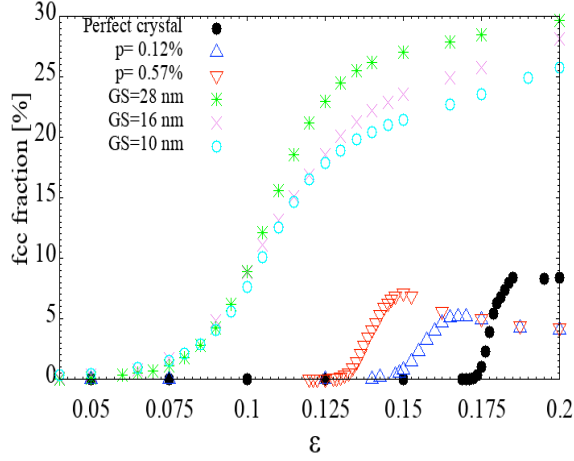


Figure 12: Evolution of the fcc atoms fraction during the compression of perfect single crystal (filled black circle); single crystal with 0.12% (up blue triangle) and 0.57% (down red triangle) of vacancy defect and polycrystalline iron with grains size (GS) of about 28 nm (green stars), 16 nm (orange cross) and 10 nm (cyan circle)

growth phase followed by a decrease and saturation after the completion of the transition.

As reported in the previous section, introducing grain boundaries makes plasticity governed by a combination of intra-grain twinning and dislocation activities from grain boundaries with small influence of elastic stiffness. Thus, the phase transition in polycrystals was found to start at a pressure of about 18 GPa and strain of 0.07 (Fig. 7) in agreement with nanosecond-laser compression experiment [3, 4] and previous MD simulations of polycrystalline iron [13, 30] (see the ref. [30] for a detailed discussion of structural phase transition for different interatomic potentials in polycrystalline iron). The hcp atoms first nucleate at grain boundaries and propagate following the twinning planes in laminar structure until the next grain boundary reached (see Fig. 11). These laminar hcp nuclei are separated by fcc planes, which atom fraction was found to be more significant than for single crystal, around 20% of atoms at the completion of the transition (see Fig. 12). Here, hcp mass fraction is clearly characterized by an initially slow variation (due to longer nucleation time) followed by a rapid growth regime which leads to the general sigmoidal shape acknowledged as a nearly universal shape of growth curves for first-order phase transformations [60]. Then, the mixed regime is found to be longer than in single crystal and span over approximately a strain variation $\Delta\varepsilon \approx 0.07$, i.e. from 0.07 to ~ 0.136 (from 18 to ~ 40 GPa). Although grain size was found to affect plasticity, no effect was found on the transition onset pressure and the hcp mass fraction evolution, probably due to saturation in the defect influence on the nucleation. On the other hand, increasing grain boundaries leads to a slight decrease in the fcc mass fraction. Here, the shear stress at the beginning of the phase transition was 4, 2.8 and 2.1 GPa for grain sizes of about 28 nm, 16 nm and 10 nm, respectively. As plasticity of polycrystalline iron is different from the single crystal case, the temperature evolution is also quite different. Temperature is found to increase linearly with the compression for polycrystalline iron with small grain sizes (about 6 to 20 nm). In contrast, for larger grains (about 30 nm), the temperature evolution during the compression is similar to that observed for single crystals, due to the significant effect of the elastic stiffening inside grains leading to a profile with two inflection points separated by

a steeper increase during the structural phase transition.

4 Conclusion

We have used non-equilibrium molecular dynamics simulations to study plasticity and phase transition in iron under uniaxial compression. Defect-free, defective (with removed atoms percentage ranging from 0.12 to 0.57% of total atoms number) [001]-oriented single crystal and polycrystalline microstructures (with grains size ranging from about 6 to 30 nm) were studied. In consistence with our previous report under piston-driven compression at lower rate [23], it is found that under uniaxial deformation both defect-free and defective iron single crystals yield via twinning that progressively recedes upon further compression while no dislocations activity is detected leading to a new increase of the deviatoric stress. Such elastic stiffening of the bcc matrix was shown to inhibit the nucleation of the hcp phase, so that the onset of the phase transformation in defect-free iron was shifted to very high pressures of about 90 GPa. Due to the rigidity of the bcc matrix, the phase transition was accompanied by a jump in the temperature resulting from the important plastic work necessary to accommodate the product phase. However, due to heterogeneous nucleation from defect the onset pressure of the phase transition was found here to be lower in defective than defect-free single crystal. The higher the defect density, the lower the onset pressure of the transition and lower the temperature growth. In the presence of grain boundaries, plasticity becomes a complex combination of intra-grain twinning and dislocation activities from grain boundaries with small influence of elastic stiffness. Then, no shift was observed in the phase transition that was found to start at around 18 GPa in consistence with the literature [3, 4, 13, 30].

Acknowledgments

Computations were performed on the supercomputer facilities of the Mésocentre de calcul de Poitou Charentes (France).

References

- [1] D. Bancroft, E. L. Peterson, and S. Minshall. Polymorphism of iron at high pressure. *J. Appl. Phys.*, 27(3):291–298, 1956.
- [2] L. M. Barker and R. E. Hollenbach. Shock wave study of the $\alpha - \varepsilon$ transition in iron. *J. Appl. Phys.*, 45(11):4872–4887, 1974.
- [3] R. F. Smith, J. H. Eggert, D. C. Swift, J. Wang, T. S. Duffy, D. G. Braun, R. E. Rudd, D. B. Reisman, J.-P. Davis, M. D. Knudson, and G. W. Collins. Time-dependence of the alpha to epsilon phase transformation in iron. *J. Appl. Phys.*, 114(22):223507, 2013.
- [4] N. Amadou, T. de Resseguier, E. Brambrink, T. Vinci, A. Benuzzi-Mounaix, G. Huser, G. Morard, F. Guyot, K. Miyanishi, N. Ozaki, R. Kodama, and M. Koenig. Kinetics of the iron $\alpha - \varepsilon$ phase transition at high-strain rates: Experiment and model. *Phys. Rev. B*, 93:214108, Jun 2016.
- [5] N. Amadou, E. Brambrink, T. de Resseguier, A. O. Manga, A. Aboubacar, B. Borm, and A. Molinari. Laser-driven ramp compression to investigate and model dynamic response of iron at high strain rates. *Metals*, 6(12), 2016.

- [6] T. de Ressaiguier and M. Hallouin. Interaction of two laser shocks inside iron samples. *J. Appl. Phys.*, 90(9):4377–4384, 2001.
- [7] T. de Ressaiguier and M. Hallouin. Effects of the α – ϵ phase transition on wave propagation and spallation in laser shock-loaded iron. *Phys. Rev. B*, 77:174107, May 2008.
- [8] D. H. Kalantar, J. F. Belak, G. W. Collins, J. D. Colvin, H. M. Davies, J. H. Eggert, T. C. Germann, J. Hawreliak, B. L. Holian, K. Kadau, P. S. Lomdahl, H. E. Lorenzana, M. A. Meyers, K. Rosolankova, M. S. Schneider, J. Sheppard, J. S. Stölken, and J. S. Wark. *Phys. Rev. Lett.*, 95:075502, 2005.
- [9] J. A. Hawreliak, B. El-Dasher, H. E. Lorenzana, G. Kimminau, A. Higginbotham, B. Nagler, S. M. Vinko, W. J. Murphy, T. Whitcher, J. S. Wark, S. Rothman, and N. Park. *In situ* x-ray diffraction measurements of the c/a ratio in the high-pressure ϵ phase of shock-compressed polycrystalline iron. *Phys. Rev. B*, 83:144114, 2011.
- [10] B. Yaakobi, T. R. Boehly, D. D. Meyerhofer, T. J. B. Collins, B. A. Remington, P. G. Allen, S. M. Pollaine, H. E. Lorenzana, and J. H. Eggert. EXAFS measurement of iron Bcc-to-Hcp phase transformation in nanosecond-laser shocks. *Phys. Rev. Lett.*, 95:075501, 2005.
- [11] Y. Ping, F. Coppari, D. G. Hicks, B. Yaakobi, D. E. Fratanduono, S. Hamel, J. H. Eggert, J. R. Rygg, R. F. Smith, D. C. Swift, D. G. Braun, T. R. Boehly, and G. W. Collins. Solid iron compressed up to 560 gpa. *Phys. Rev. Lett.*, 111:065501, Aug 2013.
- [12] K. Kadau, T. C. Germann, P. S. Lomdahl, and B. L. Holian. Atomistic simulations of shock-induced transformations and their orientation dependence in Bcc Fe single crystals. *Phys. Rev. B*, 72:064120, 2005.
- [13] K. Kadau, T. C. Germann, P. S. Lomdahl, R. C. Albers, J. S. Wark, A. Higginbotham, and B. L. Holian. Shockwaves in polycrystalline iron. *Phys. Rev. Lett.*, 98:135701, 2007.
- [14] J. Hawreliak, J. D. Colvin, J. H. Eggert, D. H. Kalantar, H. E. Lorenzana, J. S. Stölken, H. M. Davies, T. C. Germann, B. L. Holian, K. Kadau, P. S. Lomdahl, A. Higginbotham, K. Rosolankova, J. Sheppard, and J.S. Wark. Analysis of the x-ray diffraction signal for the α – ϵ transition in shock-compressed iron: Simulation and experiment. *Phys. Rev. B*, 74:184107, 2006.
- [15] K. Wang, S. Xiao, H. Deng, W. Zhu, and W. Hu. An atomic study on the shock-induced plasticity and phase transition for iron-based single crystals. *Int. J. Plast.*, 59:180 – 198, 2014.
- [16] Z. Lu, W. Zhu, T. Lu, and W. Wang. Does the Fcc phase exist in the Fe Bcc–hcp transition? a conclusion from first-principles studies. *Model. Simul. Mat. Sci. Eng.*, 22(2):025007, jan 2014.
- [17] S. J. Wang, M. L. Sui, Y. T. Chen, Q. H. Lu, E. Ma, X. Y. Pei, Q. Z. Li, and H. B. Hu. Microstructural fingerprints of phase transitions in shock-loaded iron. *Sci. Rep.*, 3:1086, 2013.
- [18] X. Cui, W. Zhu, H. He, X. Deng, and Y. Li. Phase transformation of iron under shock compression: Effects of voids and shear stress. *Phys. Rev. B*, 78:024115, Jul 2008.
- [19] T. de Ressaiguier and M. Hallouin. Stress relaxation and precursor decay in laser shock-loaded iron. *J. Appl. Phys.*, 84(4):1932–1938, 1998.

- [20] B. J. Jensen, G. T. Gray, and R. S. Hixson. Direct measurements of the α - ϵ transition stress and kinetics for shocked iron. *J. Appl. Phys.*, 105:103502, 2009.
- [21] R. F. Smith, J. H. Eggert, R. E. Rudd, D. C. Swift, C. A. Bolme, and G. W. Collins. High strain-rate plastic flow in Al and Fe. *J. Appl. Phys.*, 110(12):123515, 2011.
- [22] A. Higginbotham, M. J. Suggit, E. M. Bringa, P. Erhart, J. A. Hawreliak, G. Mogni, N. Park, B. A. Remington, and J. S. Wark. Molecular dynamics simulations of shock-induced deformation twinning of a body-centered-cubic metal. *Phys. Rev. B*, 88:104105, Sep 2013.
- [23] N. Amadou, T. de Resseguier, A. Dragon, and E. Brambrink. Coupling between plasticity and phase transition in shock- and ramp-compressed single-crystal iron. *Phys. Rev. B*, 98:024104, Jul 2018.
- [24] J. Li, Q. Wu, J.D. Yu, Y. Tan, S.L. Yao, T. Xue, and K. Jin. Orientation effect of alpha-to-epsilon phase transformation in single-crystal iron. *Acta Phys. Sin.*, 66(12):146201, 2017.
- [25] T. Mashimo, M. Uchino, A. Nakamura, T. Kobayashi, E. Takasawa, T. Sekine, Y. Noguchi, H. Hikosaka, K. Fukuoka, and Y. Syono. Yield properties, phase transition, and equation of state of aluminum nitride (AlN) under shock compression up to 150 gpa. *J. Appl. Phys.*, 86(12):6710–6716, 1999.
- [26] L. Wu, K. Wang, S. Xiao, H. Deng, W. Zhu, and W. Hu. Atomistic studies of shock-induced phase transformations in single crystal iron with cylindrical nanopores. *Comput. Mater. Sci.*, 122:1 – 10, 2016.
- [27] N. Gunkelmann, E. M. Bringa, D. R. Tramontina, C. J. Ruestes, M. J. Suggit, A. Higginbotham, J. S. Wark, and H. M. Urbassek. Shock waves in polycrystalline iron: Plasticity and phase transitions. *Phys. Rev. B*, 89:140102, 2014.
- [28] X. Zhang, K. Wang, W. Zhu, J. Chen, M. Cai, S. Xiao, H. Deng, and W. Hu. Effect of grain boundaries on shock-induced phase transformation in iron bicrystals. *J. Appl. Phys.*, 123(4):045105, 2018.
- [29] Y. Huang, Y. Xiong, P. Li, X. Li, S. Xiao, H. Deng, W. Zhu, and W. Hu. Atomistic studies of shock-induced plasticity and phase transition in iron-based single crystal with edge dislocation. *Int. J. Plast.*, 114:215 – 226, 2019.
- [30] N. Gunkelmann, E. M. Bringa, K. Kang, G. J. Ackland, C. J. Ruestes, and H. M. Urbassek. Polycrystalline iron under compression: Plasticity and phase transitions. *Phys. Rev. B*, 86:144111, 2012.
- [31] K. Wang, W. Zhu, S. Xiao, K. Chen, H. Deng, and W. Hu. Coupling between plasticity and phase transition of polycrystalline iron under shock compressions. *Int. J. Plast.*, 71:218 – 236, 2015.
- [32] K. Wang, J. Chen, X. Zhang, and W. Zhu. Interactions between coherent twin boundaries and phase transition of iron under dynamic loading and unloading. *J. Appl. Phys.*, 122(10):105107, 2017.

- [33] N. Amadou, T. De Resseguier, A. Dragon, and E. Brambrink. Effects of orientation, lattice defects and temperature on plasticity and phase transition in ramp-compressed single crystal iron. *Comput. Mater. Sci.*, 172:109318, 2020.
- [34] B. T. Wang, J. L. Shao, G. C. Zhang, W. D. Li, and P. Zhang. Molecular dynamics simulations of hcp/fcc nucleation and growth in bcc iron driven by uniaxial compression. *J. Phys. Condens. Matter*, 21(49):495702, nov 2009.
- [35] S. Plimpton. Fast parallel algorithms for short-range molecular dynamics. *J. Comp. Phys.*, 117:1–19, 1995.
- [36] M. S. Daw and M. I. Baskes. Semiempirical, quantum mechanical calculation of hydrogen embrittlement in metals. *Phys. Rev. Lett.*, 50:1285–1288, 1983.
- [37] S. M. Foiles, M. I. Baskes, and M. S. Daw. Embedded-atom-method functions for the fcc metals Cu, Ag, Au, Ni, Pd, Pt, and their alloys. *Phys. Rev. B*, 33:7983–7991, 1986.
- [38] N. Gunkelmann, D. R. Tramontina, E. M. Bringa, and H. M. Urbassek. Interplay of plasticity and phase transformation in shock wave propagation in nanocrystalline iron. *New J. Phys.*, 16(9):093032, 2014.
- [39] P. Hirel. AtomsK: A tool for manipulating and converting atomic data files. *Comput. Phys. Comm.*, 197:212 – 219, 2015.
- [40] J. C. Crowhurst, B. W. Reed, M. R. Armstrong, H. B. Radousky, J. A. Carter, D. C. Swift, J. M. Zaug, R. W. Minich, N. E. Teslich, and M. Kumar. The $\alpha - \epsilon$ phase transition in iron at strain rates up to $10^9 s^{-1}$. *J. Appl. Phys.*, 115(11):113506, 2014.
- [41] J. L. Shao, S. Q. Duan, A. M. He, C. S. Qin, and P. Wang. Dynamic properties of structural transition in iron under uniaxial compression. *J. Phys. Condens. Matter.*, 21(24):245703, may 2009.
- [42] O. Guerrero and M. Marucho. Elastic-plastic transition under uniaxial stress bcc tantalum. *Journal of Materials Science and Engineering B*, 3(3):153, March 2013.
- [43] J.-L. Shao, P. Wang, F.-G. Zhang, and A.-M. He. Effects of temperature and void on the dynamics and microstructure of structural transition in single crystal iron. *Journal of Physics: Condensed Matter*, 30(25):255401, may 2018.
- [44] A. Stukowski. Visualization and analysis of atomistic simulation data with OVITO—the open visualization tool. *Model. Simul. Mat. Sci. Eng.*, 18(1):015012, dec 2009.
- [45] A. Stukowski, V. V. Bulatov, and A. Arsenlis. Automated identification and indexing of dislocations in crystal interfaces. *Modelling and Simulation in Materials Science and Engineering*, 20(8):085007, oct 2012.
- [46] A. Stukowski. Structure identification methods for atomistic simulations of crystalline materials. *Modelling and Simulation in Materials Science and Engineering*, 20(4):045021, may 2012.
- [47] M. A. Meyers. *Dynamic behavior of materials*. 1994. pp: 1.

- [48] L. A. Zepeda-Ruiz, A. Stukowski, T. Oettel, and V. V. Bulatov. Probing the limits of metal plasticity with molecular dynamics simulations. *Nature*, 550:492, 2017.
- [49] In the limit of validity of the interatomic potential.
- [50] H.-T. Luu and N. Gunkelmann. Pressure-induced phase transformations in Fe-C: Molecular dynamics approach. *Comput. Mater. Sci.*, 162:295 – 303, 2019.
- [51] R. E. Smallman and A. H. W. Ngan. *Modern Physical Metallurgy*. Elsevier, 2014.
- [52] J. W. Christian. *The Theory of Transformations in Metals and Alloys*. Elsevier, 2002. pp: 464.
- [53] M. Avrami. Kinetics of phase change. I general theory. *J. Chem. Phys.*, 7:1103–1112, July 1939.
- [54] M. Avrami. Kinetics of phase change. II transformation time relations for random distribution of nuclei. *J. Chem. Phys.*, 7:212–224, Feb. 1940.
- [55] D.J. Andrews. Calculation of mixed phases in continuum mechanics. *J. Comput. Phys.*, 7(2):310 – 326, 1971.
- [56] J.C. Boettger and D. C. Wallace. Metastability and dynamics of the shock-induced phase transition in iron. *Phys. Rev. B*, 55:2840–2849, Feb 1997.
- [57] M. Bastea, S. Bastea, and R. Becker. High pressure phase transformation in iron under fast compression. *Appl. Phys. Lett.*, 95:241911, Dec. 2009.
- [58] K. Kadau, T. C. Germann, P. S. Lomdahl, and B. L. Holian. Shock-induced structural phase transformations studied by large-scale molecular-dynamics simulations. *AIP Conf. Proceedings*, 620(1):351–354, 2002.
- [59] J.-L. Shao, S. Q. Duan, A. M. He, P. Wang, and C. S. Qin. Microscopic dynamics of structural transition in iron with a nanovoid under shock loading. *Journal of Physics: Condensed Matter*, 22(35):355403, aug 2010.
- [60] N. Hamaya, Y. Yamada, J. D. Axe, D. P. Belanger, and S. M. Shapiro. Neutron scattering study of the nucleation and growth process at the pressure-induced first-order phase transformation of RbI. *Phys. Rev. B*, 33:7770–7776, Jun 1986.